

# A Numerical Study of Backscattering From Time-Evolving Sea Surfaces: Comparison of Hydrodynamic Models

Joel T. Johnson, *Member, IEEE*, Jakov V. Toporkov, *Associate Member, IEEE*, and Gary S. Brown, *Fellow, IEEE*

**Abstract**—Results from a Monte Carlo simulation of backscattering from one-dimensional (1-D) time-evolving sea surface models are reported. A numerical electromagnetic method based on an accelerated forward-backward approach is used to calculate backscattered returns from impedance surface profiles at incidence angles of  $0^\circ$  (normal),  $40^\circ$ , and  $80^\circ$ . Surfaces are initialized as realizations of a Pierson-Moskowitz spectrum and then stepped in time through a numerical hydrodynamic method. Results from three distinct hydrodynamic methods are compared: a linear evolution, the “improved linear representation” of Creamer *et al.* [7], and the “Watson-West” approach of West *et al.* in [8]. Instabilities in the West model due to formation of steep wave features limit the study to L-band backscattering for wind speeds less than 2 m/s, so that the surfaces considered are only slightly rough on an electromagnetic scale. The small slope approximation for electromagnetic scattering is shown to provide reasonable predictions in this limit. Statistics of the resulting surface profiles and backscattered fields are compared for the three models and are found to be similar in most respects. Backscattered field Doppler spectra, however, show differences, with the West model apparently capturing more nonlinear interactions in the surface evolution.

**Index Terms**—Doppler spectrum, rough surface scattering, sea scattering.

## I. INTRODUCTION

RECENT improvements in computing technologies and in numerical algorithms for scattering from rough surfaces are now making large scale numerical studies of scattering from ocean-like surfaces possible. Several recent works have explored average scattering cross sections for one-dimensional (1-D) surfaces (i.e., having roughness in only one horizontal direction) through Monte Carlo simulations using time-independent linear models of the sea surface [1]. Time variations of the sea surface, however, cause backscattered field returns to be spread into a

Manuscript received September 27, 2000; revised August 10, 2001. This work was sponsored by ONR Contracts N00014-97-1-0541 and N00014-00-1-0399 and the Maui High Performance Computing Center, Maui, HI, for use of the IBM SP system, which is sponsored by the Air Force Research Laboratory, Air Force Materiel Command, under Cooperative Agreement F29601-93-2-0001. Opinions, interpretations, conclusions, and recommendations are those of the authors and are not necessarily endorsed by the United States Air Force, Air Force Research Laboratory, or the U.S. Government.

J. T. Johnson is with the Department of Electrical Engineering and ElectroScience Laboratory, The Ohio State University, Columbus, OH 43210 USA (e-mail: johnson@ee.eng.ohio-state.edu).

J. V. Toporkov is with SFA, Inc., Largo, MD, and is also with the Naval Research Laboratory, Washington, DC, USA.

G. S. Brown is with the Bradley Department of Electrical and Computer Engineering, Virginia Polytechnic Institute, Blacksburg, VA 24061 USA.

Publisher Item Identifier S 0196-2892(01)10398-0.

Doppler spectrum so that average Doppler spectra are also of interest for sea surface scattering. Prediction of sea surface Doppler spectra requires a Monte Carlo simulation in which scattering calculations are performed at a series of time steps as surface realizations evolve. Although several studies of scattering from surfaces rough in two dimensions have also been reported (for example [2], [3]), the requirement of repeated calculations for multiple realizations at multiple time steps prevents Doppler studies with two-dimensional (2-D) surfaces at present.

References [4]–[6] have applied numerical scattering models for 1-D sea surfaces and included time variations to investigate scattered field time statistics. Reference [6] concentrated on forward scattered fields and used only a linear model of surface evolution, while [4] and [5] focus on backscattering and consider both linear evolution and the “improved linear representation” of [7]. Results in [5] show significant differences for L-band Doppler spectra at wind speed 5 m/s, with the linear and Creamer models [7].

In this paper, the studies of [5] are continued to further explore the influence of the hydrodynamic model on L-band backscattered field statistics. An additional hydrodynamic model, that of the West model [8], is included in the study. The three hydrodynamic models used are described in Section II, along with a comparison of surface statistics from the Monte Carlo simulation. Unlike [5], the study is limited to maximum wind speeds of 2 m/s due to stability limitations of the West model. Although 2 m/s is very low when compared to global mean sea wind speeds, the results obtained still demonstrate the importance of nonlinear hydrodynamic interactions and the influence of the hydrodynamic model used. Because the resulting surfaces are only slightly rough on an electromagnetic scale, approximate electromagnetic scattering models may be applicable. Section III describes the numerical electromagnetic scattering model used and also discusses the small slope approximation (SSA) [9], which is later used to compare with numerical scattering model results. Section IV compares backscattered field statistics and Doppler spectra obtained from the simulation under both the numerical and SSA scattering models for the three hydrodynamic approaches. Final conclusions are presented in Section V.

## II. HYDRODYNAMIC METHODS

Hydrodynamic evolution of the surface  $z = h(x, t)$  of an irrotational, incompressible fluid is described by a pair of coupled

nonlinear hydrodynamic equations [8]

$$\frac{\partial h}{\partial t} = \frac{\partial \phi}{\partial z} \left[ 1 + \left( \frac{\partial h}{\partial x} \right)^2 \right] - \frac{\partial h}{\partial x} \frac{\partial \phi}{\partial x} \quad (1)$$

$$\frac{\partial \phi}{\partial t} = -gh - \frac{1}{2} \left( \frac{\partial \phi}{\partial x} \right)^2 + \frac{1}{2} \left( \frac{\partial \phi}{\partial z} \right)^2 \left[ 1 + \left( \frac{\partial h}{\partial x} \right)^2 \right] \quad (2)$$

where  $\phi$  is the velocity potential evaluated at the surface,  $g$  is the acceleration of gravity, and  $x$  and  $t$  are spatial (horizontal) and time coordinates, respectively. These equations form a canonical pair derivable from a single Hamiltonian and thus conserve energy contained in the initial values of  $h$  and  $\phi$ , which begin the simulation. Note surface tension is not included in the previous equations due to limitations of the [7] method, which applies only for gravity wave evolution. This fact limits the current study to L-band backscattering, for which surface tension can be neglected in the Bragg scattering region, as discussed in [5].

Since an exact solution to these equations for a general initial condition is not known, either approximate or numerical methods are required for surface time evolution. Numerical solution of (1)–(2) through a time-stepping process is susceptible to instability and must be performed carefully. Furthermore, computation of the  $\partial\phi/\partial z$  term can be difficult if values of  $\phi$  are known only on the interface. The three methods used for the study are described in the following. Note in all these methods, a uniform grid is used for description of  $h$  and  $\phi$ , so that overturning features cannot be captured. Methods based on a boundary integral approach [10], [11] avoid many of these problems but also have substantially greater computational requirements than those available for the current study.

#### A. Linear Evolution

If nonlinear terms are neglected, (1)–(2) can be solved analytically to determine  $h$  and  $\phi$  as a set of independent waves propagating according to the gravity wave dispersion relationship

$$h(x, t) = \frac{1}{2\pi} \int dk_x \tilde{h}(k_x) \exp[-i(k_x x - \omega t)] \quad (3)$$

$$\phi(x, t) = \frac{1}{2\pi} \int dk_x i \frac{\omega}{k_x} \tilde{h}(k_x) \exp[-i(k_x x - \omega t)] \quad (4)$$

$$= \frac{1}{2\pi} \int dk_x \tilde{\phi}(k_x) \exp[-i(k_x x - \omega t)] \quad (5)$$

where  $\omega = \text{sgn}(k_x) \sqrt{g|k_x|}$  is the gravity wave dispersion relation, and  $\text{sgn}(x)$  is the sign of  $x$  defined as +1 for  $x$  positive, -1 for  $x$  negative. The function  $\tilde{h}(k_x)$  in (3) satisfies  $\tilde{h}(k_x) = \tilde{h}^*(-k_x)$ , where  $*$  denotes the complex conjugate operation, to insure that  $h(x, t)$  is real. Note all waves in the above equations are assumed to propagate in the positive  $x$  direction. Given an initial profile  $h(x, 0)$ , a Fourier transform operation can be performed to determine  $\tilde{h}(k_x)$ , and a phase shifting operation followed by an inverse Fourier transform is all that is required to obtain  $h(x, t)$ . Because all Fourier components of the surface propagate independently in the linear model, amplitudes of a given surface Fourier component remain fixed for all times.

Discretized surfaces  $h(x, t)$  of length  $L$  in the linear model are generated as realizations of a Pierson–Moskowitz spectrum through

$$h(x, t) = \frac{1}{L} \sum_n \tilde{h}(k_{xn}) \exp[-i(k_{xn}x - \omega_n t)] \quad (6)$$

$$\tilde{h}(k_{xn}) = \frac{\gamma_n}{\sqrt{2}} \sqrt{2\pi L} \sqrt{W(k_{xn})} \quad n \geq 0 \quad (7)$$

$$\tilde{h}(k_{xn}) = \tilde{h}(k_{x(-n)})^* \quad n < 0 \quad (8)$$

$$W(k_{xn}) = \frac{0.0081}{4k_{xn}^3} \exp\left\{-\frac{0.74g^2}{k_{xn}^2 U^4}\right\} \quad (9)$$

where  $\gamma_n$  is a complex random number whose real and imaginary parts are samples of a Gaussian random variable with mean zero and unit variance,  $k_{xn} = (2\pi n)/L$ ,  $\omega_n = \text{sgn}(k_{xn}) \sqrt{g|k_{xn}|}$ ,  $g$  is the acceleration of gravity 9.81 m/s<sup>2</sup>, and  $U$  is the wind speed in m/s (here 2 m/s). The spectrum  $W(k_{xn})$  given earlier is defined so that the integral over all positive and negative  $k_{xn}$  values yields a surface height variance of  $(2.74 \times 10^{-3})U^4/g^2$ , as expected for a Pierson–Moskowitz spectrum. The surface generation procedure described is identical to that of [5], although a different definition is used for the spectrum and for the variances of the complex numbers  $\gamma_n$  in the reference.

#### B. “Improved Linear” Representation

In [7], Creamer *et al.* derive an “improved linear representation” for gravity wave surfaces by performing a canonical transformation of variables in the hydrodynamic equations. The new variables  $h'$  and  $\phi'$  do not represent the actual surface height displacement and velocity potential but are advantageous because the transformation is derived such that the first nonlinear term in the Hamiltonian of the new variables vanishes. The equations of motion for the transformed variables are then approximated as linear so that  $h'$  and  $\phi'$  evolve according to (3)–(5) and no numerical time stepping is required. Initial values of  $h'$  and  $\phi'$  are also obtained as realizations of a Pierson–Moskowitz spectrum. The actual surface height  $h$  is obtained from a nonlinear integration over  $h'$  as described in [5] and has been demonstrated to contain nonlinear features in [7]. However, surfaces obtained in this model are found to contain vertical but no horizontal deviations from the underlying linear profile  $h'$  due to the linear evolution approximation for  $h'$ . Also, the integration to obtain  $h$  from  $h'$  requires an  $O(N^2)$  operation, where  $N$  is the number of points in the surface profile, so the [7] model can become computationally expensive for large  $N$ . However, the model never has stability problems since it does not require numerical time stepping.

#### C. The West Model

The final method considered is that of [8], which numerically time steps (1)–(2) given initial values  $h(x, 0)$  and  $\phi(x, 0)$ . The method determines  $\partial\phi/\partial z$  from values of  $\phi$  on the interface through the “Watson–West” expansion in surface slope derived in [12]. The zeroth term in the expansion is expressed in the spectral domain as  $|k_x| \tilde{\phi}(k_x)$  (from which the linearly propagating solution (3)–(5) is obtained), while higher order terms

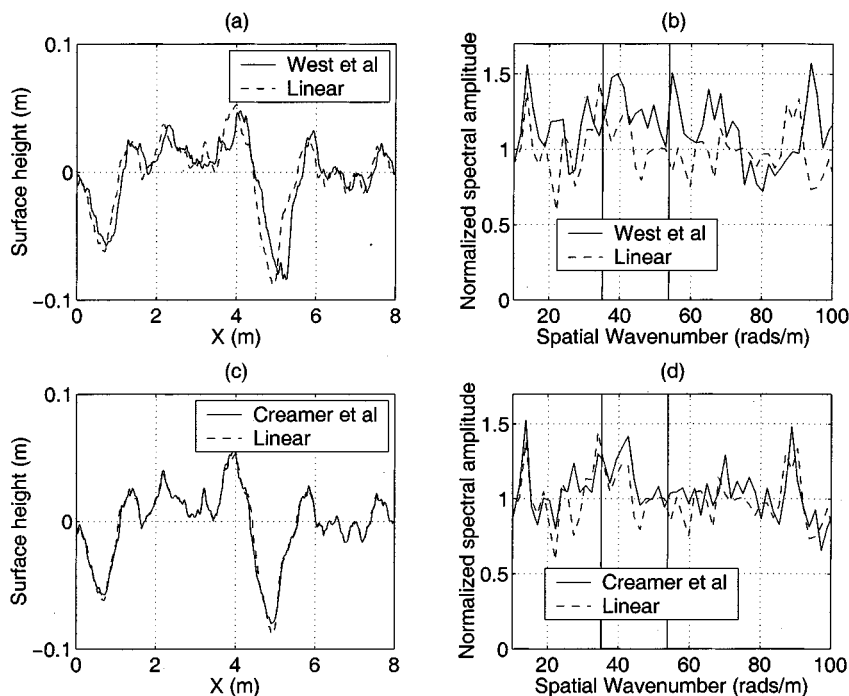


Fig. 1. Comparison of surface profiles and normalized spectra for a single surface realization for (a) the West model and linear model profiles, (b) the West model and linear model spectra, (c) the Creamer and linear model profiles, and (d) the Creamer and linear model spectra.

involve higher order powers of  $\phi(x, t)$  and  $h(x, t)$ . Thus, for a given “order”  $M$  of the Watson–West method, terms of higher order than  $h^n \phi^{M+1-n}$  for  $n = 0$  to  $M + 1$  are neglected. Note that sampling requirements in the method are increased as  $M$  increases as described in [8] in order to avoid spectral aliasing effects. The “high order spectral method” [13] for hydrodynamic evolution of a surface is an equivalent hydrodynamic technique based on a similar expansion, but uses a different method to avoid aliasing problems.

A fourth-order Adams–Bashforth predictor-corrector algorithm [14] is used to time step (1)–(2) and is initialized again with a realization of a Pierson–Moskowitz spectrum which is assumed to be propagating linearly at previous time steps according to (3)–(5). To avoid introducing discontinuities into the time evolution, an initial “ramp-up” period is included in the simulation, during which all nonlinear terms in (1)–(2) and in the expansion of  $\partial\phi/\partial z$  have their amplitudes multiplied by

$$R(t) = \exp \left[ - \left( \frac{t-a}{b} \right)^2 \right] \quad (10)$$

for  $t < a$ , where  $a$  and  $b$  are constants in seconds. For a simulation beginning at  $t = 0$ , appropriate choices of  $a$  and  $b$  result in an initial linear evolution so that the linear initialization of the time-stepping algorithm is appropriate. As time  $t = a$  is approached, nonlinear hydrodynamic effects are gradually increased, and  $R(t)$  remains unity for  $t > a$ . This “adiabatic bootstrapping” procedure is similar to that discussed in [8] and [15], and should not overly influence final surface properties for reasonable choices of  $a$  and  $b$ . Variations with these parameters are considered in Section IV.

The West model computationally is an  $O(N \log N)$  method due to use of the fast Fourier transform (FFT) in evaluating

$\partial\phi/\partial z$ . The method can also be extended to 2-D surfaces and to include surface tension effects and approximate wind forcing and viscosity effects [16]. However, the West model is susceptible to instability problems and breaks down when steep features in the surface are formed due to the slope expansion involved. Sampling requirements can also become stringent as the order  $M$  is increased. For the studies of this paper, fourth-order ( $M = 4$ ) calculations failed for a large fraction of surface realizations when wind speeds were increased beyond 2 m/s due to formation of steep features in the short wave portion of the spectrum. Although inclusion of artificial viscosity terms in the short wave portion of the spectrum or use of additional filtering [13] could potentially reduce these problems, a desire to avoid additional physical approximations prevents use of these steps in the current study. Results in the following sections at wind speed 2 m/s will still illustrate the importance of nonlinear hydrodynamic interactions and the influence of the hydrodynamic model applied.

#### D. Computational Issues

The studies of this paper are similar to those of [5], and involve electromagnetic scattering at  $\lambda = 23$  cm wavelength at incidence angles of  $0^\circ$  (normal incidence),  $40^\circ$ , and  $80^\circ$ . A surface size of 117.81 m  $\approx 512.2\lambda$  was chosen for all cases in order to avoid any surface edge scattering effects at the largest incidence angle as discussed further in Section III. Since the peak wave of the Pierson–Moskowitz spectrum at wind speed 2 m/s is approximately 3.6-m long, a large number of peak wavelengths are resolved in a single surface realization. The Bragg scattering region for  $k_0 = (2\pi)/(\lambda)$  includes spatial frequencies up to  $2k_0$ , so a high spatial frequency cutoff of  $k_h = 109$  rads/m ( $\approx 4k_0$ ) was used in the simulation. This high-frequency cutoff is maintained in the West model through an ideal low pass filter which

is applied at each time step to the right hand sides of (1)–(2). An electromagnetic sampling rate of approximately  $\Delta x = \lambda/16$  results in a total of 8192 points in scattering calculations for each realization. The linear and Creamer models also use 8192 points in the hydrodynamic simulation, while the fourth order the West model oversamples the profile to 16 384 points to avoid aliasing problems. A time duration of 5.12 s for scattering results is used as in [5] in order to obtain sufficient Doppler spectral resolution, and scattering results are calculated every 0.02 s to obtain sufficient unambiguous Doppler bandwidth. Since the linear and Creamer model time evolution is exact, use of 0.02 s as the surface evolution time step does not cause problems, but a finer time step of 0.004 s is required in the numerical time stepping the West model to retain accuracy. Ramp-up parameters  $a$  and  $b$  are set to 1 and 0.376 s, respectively, in the West model. Scattering calculations do not begin until  $t = a$  when the ramp period is over, so a total surface evolution time of 6.12 s is obtained. Linear model and the “underlying” linear surface of the Creamer method are equal to those of the West model at time  $t = 0$ , and are also evolved for one second before scattering calculations begin.

Computations for the study were performed using IBM SP parallel computing resources at the Maui High Performance Computing Center (MHPCC), Maui, HI [17], with Monte Carlo simulations performed in parallel simply by running distinct surface realizations on distinct nodes of the system. Individual realization, single time step computational times were comparable to those reported in [5] and remain dominated by the electromagnetic calculations due to the multiple incidence angles and polarizations used. Hydrodynamic model computing times with the West model were found to be approximately one half of those with the Creamer model, even with the larger number of surface points, finer time step, and fourth order calculations, indicating the advantages of an  $O(N \log N)$  method. A set of 96 initial profiles was used in the Monte Carlo simulation (performed in 3–32 processor runs), but the West model failed for 14 of these profiles due to the formation of steep features in the short wave portion of the spectrum. Final results for all three hydrodynamic methods thus include only the 82 profiles that completed the West model evolution. Convergence tests of the resulting data show that reasonable statistics are obtained from this number of realizations. The influence of the eliminated 14 profiles on average results is difficult to assess, but is not believed to be extreme due to the moderate fraction of unstable profiles and the low wind speeds considered. Note the comparison of hydrodynamic methods and scattering results is not influenced at all since results are compared for an identical set of profiles.

### E. Comparison of Surfaces

Fig. 1 illustrates a comparison of surface profiles (only an 8-m portion of the total 117.81 m length is shown) and corresponding normalized surface spectra (the power spectral density of the surface divided by the Pierson–Moskowitz spectrum) for a sample surface realization upon completion of the 6.12 s evolution. The profile comparisons in plots (a) and (c) show the West model obtains a larger deviation from the linear profile than the [7] model. Note the latter yields noticeable deviations

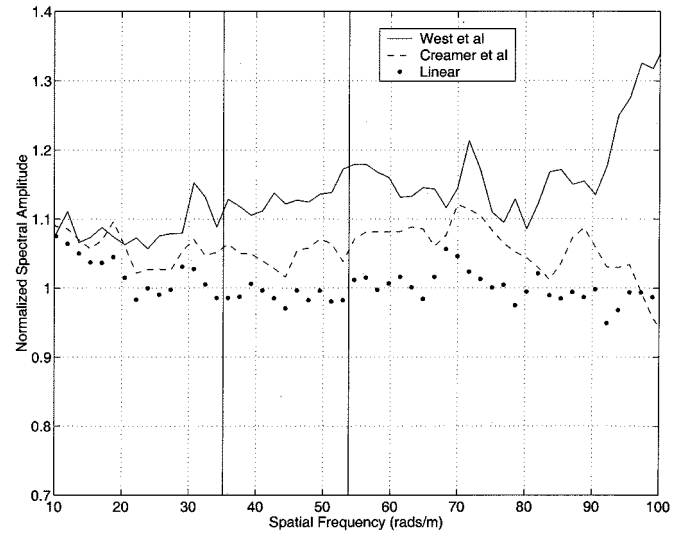


Fig. 2. Comparison of average normalized spectra.

TABLE I  
AVERAGE NORMALIZED RADAR CROSS SECTIONS

Incidence angle	pol	RCS (dB) West	RCS (dB) Creamer	RCS (dB) linear	RCS (dB) SPM (linear)
0	VV	15.84	15.69	15.69	N/A
40	VV	-22.93	-23.04	-23.04	-23.42
80	VV	-31.27	-31.83	-31.83	-31.91
0	HH	15.99	15.94	15.92	N/A
40	HH	-28.70	-29.05	-29.34	-31.91
80	HH	-56.98	-58.16	-59.15	-60.47

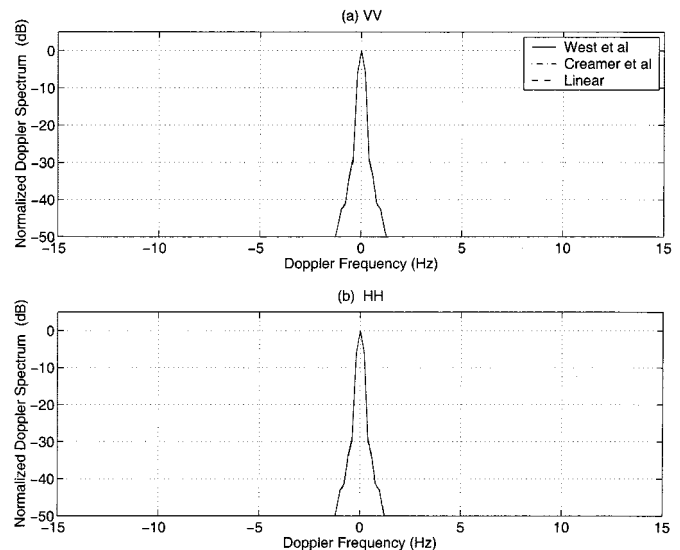


Fig. 3. Comparison of Doppler spectra for  $0^\circ$  incidence (a) VV and (b) HH.

primarily at peaks and troughs of waves, with no horizontal shift in the profile as expected. Normalized spectra in plots (b) and (d) were estimated using a 256 point periodogram method as described in [14] and show somewhat larger deviations from linear results with the West model; the vertical lines in these plots indicate the Bragg wavenumbers at  $40^\circ$  and  $80^\circ$  incidence.

Statistics of the set of 82 final profiles can also be compared for the three models. Standard deviations averaged over all 82 realizations are  $\sigma = 2.13, 2.14,$  and  $2.15$  cm for the West model,

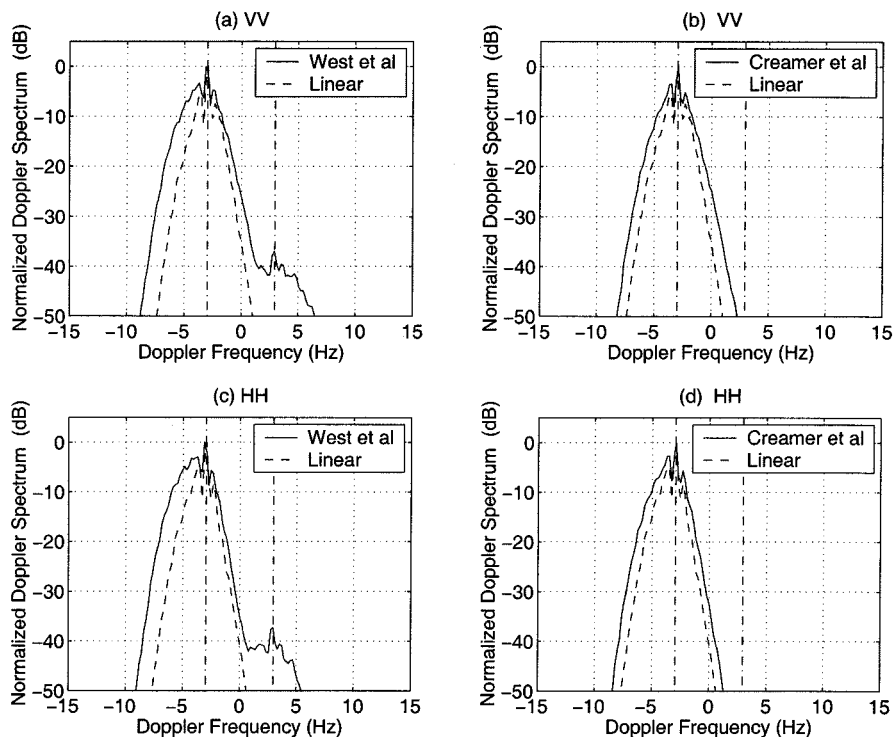


Fig. 4. Comparison of Doppler spectra for  $40^\circ$  incidence (a) VV, West model, and linear, (b) VV, Creamer model, and linear, (c) HH, West model, and linear, and (d) HH, Creamer model, and linear.

Creamer model, and linear models, respectively, compared to the analytical 2.13 cm for the Pierson–Moskowitz spectrum at 2 m/s. This 1% variation in root mean square (rms) height between the three methods is not significant for an ensemble of 82 surface realizations. Surface height and slope histograms with the entire set of realizations for each model were found to be well fit by a Gaussian approximation, indicating that surface horizontal asymmetries caused by nonlinear interactions are not statistically significant at wind speed 2 m/s. Average spectra normalized to the Pierson–Moskowitz spectrum are illustrated in Fig. 2 and show a general increase in high-frequency content of the surface spectrum moving from the linear to the Creamer model to the West model. The vertical lines in the figure again indicate the Bragg wavenumbers for  $40^\circ$  and  $80^\circ$  incidence. Although these statistics indicate some differences between the three models, the results basically support a Gaussian random process surface model for all three hydrodynamic methods, with only slightly different spectra and height standard deviations. Although these differences influence scattering results, comparisons of backscattered field Doppler spectra in Section IV show larger differences than would be expected from these final profile statistics, indicating the importance of the detailed temporal evolution process on scattered field Doppler spectra.

### III. SCATTERING MODELS

The numerical electromagnetic scattering model applied is a standard integral equation algorithm for 1-D impedance surfaces, with an iterative matrix equation solver based on the forward-backward algorithm [18]. Calculations are accelerated to

order  $N$  through the spectral domain method described in [19], [20]. A tapered wave incident field is used with  $g = 6$  to avoid surface edge scattering effects, and a surface size of  $512.2\lambda$  is chosen to allow accurate calculations to  $80^\circ$  incidence following the guidelines of [21]. The surface permittivity at  $\lambda = 23$  cm is taken as  $76 + i53$  from the model of [22].

Since an rms height of approximately 2.15 cm results in a  $k_0\sigma$  product of 0.59, the surfaces considered are only slightly rough on an electromagnetic scale. This fact motivates a comparison of numerical results with those from more approximate scattering models. The small slope approximation [9] is chosen for this purpose, and is implemented for deterministic surfaces and applied in the Monte Carlo simulation following the formulations of [23], [24]. Both first and second-order SSA fields are considered. First-order SSA results are identical in the perfectly conducting surface limit to the model of [25] for backscattering, as discussed in [26], and produce no difference in the frequency dependence of horizontal (HH) and vertical (VV) polarized Doppler spectra. Second-order SSA results provide a polarization sensitive correction but require additional computations; analysis of the second-order SSA theory [27] has shown that the composite surface theory [28] is obtained in the limit of a true two scale surface. Although  $k_0\sigma = 0.59$  is somewhat outside the validity range of the first order small perturbation method (SPM) [29], the Bragg scattering relationship between a single component of the surface spectrum and scattered fields can remain a basic guideline for examining electromagnetic results, particularly at  $\theta_i = 80^\circ$  incidence where the surface scattering Rayleigh parameter (which is proportional to  $\cos\theta_i$ ) is reduced. Evidence of Bragg scattering at this incidence angle will be discussed in the next section.

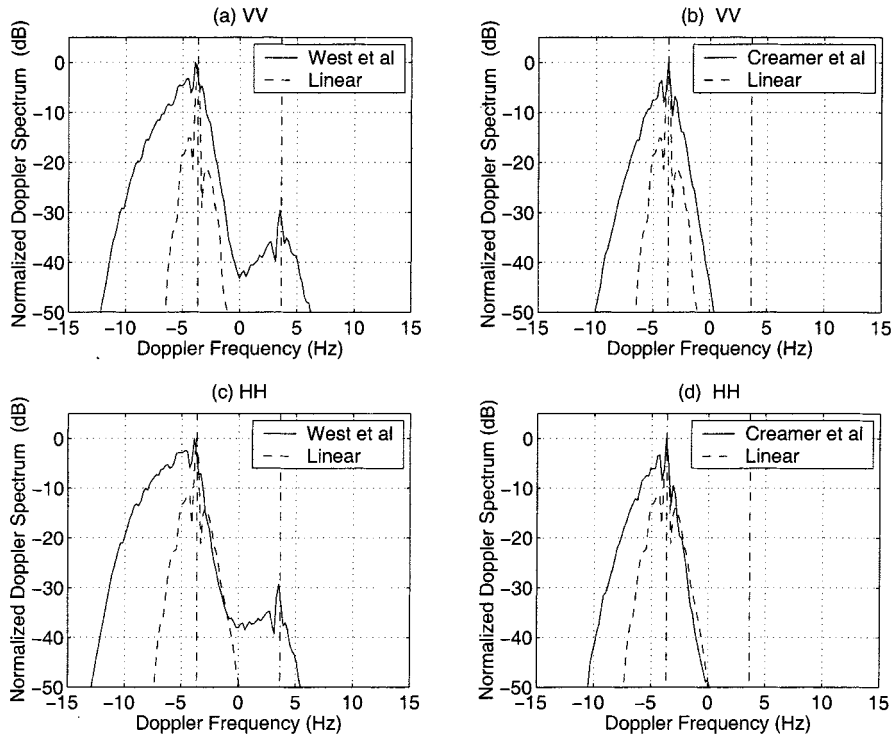


Fig. 5. Comparison of Doppler spectra for  $80^\circ$  incidence (a) VV, West model, and linear, (b) VV, Creamer model, and linear, (c) HH, West model, and linear, and (d) HH, Creamer model, and linear.

TABLE II  
DOPPLER SPECTRA FIRST MOMENTS

Incidence angle	pol	Mean freq (Hz)			Bragg freq (Hz)
		West	Creamer	Linear	
40	VV	-3.46	-3.20	-3.06	-2.95
80	VV	-4.62	-4.11	-3.71	-3.66
40	HH	-3.83	-3.46	-3.30	-2.95
80	HH	-5.28	-4.44	-3.74	-3.66

#### IV. RESULTS

Statistics of backscattered fields for the entire set of realizations and time samples were first examined. Table I presents the average normalized radar cross sections (RCS)  $\sigma_{hh}^0$  and  $\sigma_{vv}^0$  for the three hydrodynamic models at  $\theta_i = 0^\circ, 40^\circ$ , and  $80^\circ$  incidence, and for comparison includes predictions from the SPM at oblique angles. SPM results were computed from

$$\sigma_{hh}^0 = 4k^3 \cos^4 \theta_i W(2k \sin \theta_i) |\Gamma_h|^2 \quad (11)$$

$$\sigma_{vv}^0 = \sigma_{hh}^0 \left| \frac{\cos \theta_i + \sqrt{\epsilon - \sin^2 \theta_i}}{\epsilon \cos \theta_i + \sqrt{\epsilon - \sin^2 \theta_i}} \right|^4 |\sin^2 \theta_i (\epsilon - 1) + \epsilon|^2 \quad (12)$$

where

$$\Gamma_h = \frac{\cos \theta_i - \sqrt{\epsilon - \sin^2 \theta_i}}{\cos \theta_i + \sqrt{\epsilon - \sin^2 \theta_i}} \quad (13)$$

is the Fresnel reflection coefficient for horizontal polarization evaluated at angle  $\theta_i$ ,  $k = (2\pi)/(\lambda)$  is the electromagnetic wavenumber for incident electromagnetic wavelength  $\lambda$ , and  $\epsilon$  is the relative permittivity of the surface.

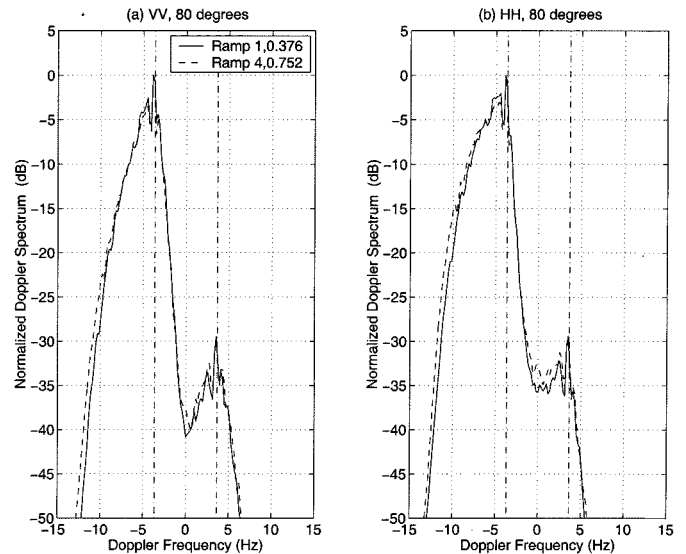


Fig. 6. Effect of "ramp-up" parameters on the West model, Doppler spectra at  $80^\circ$  (a) VV and (b) HH.

Results show that all three models yield comparable scattering cross sections, except in HH polarization at  $80^\circ$  incidence, where the West model and [7] model results are increased over those of linear surfaces. The increase of approximately 2.17 dB in HH polarization at  $80^\circ$  from the linear to the West model is somewhat larger than but comparable to the increase of approximately 0.7 dB observed in the spectra of Fig. 2 at the Bragg wavenumber. RCS values from the SPM are within 0.4 dB of linear hydrodynamic model results for VV polarization, but underestimate HH results by 2.6 and 1.3 dB at  $40^\circ$  and  $80^\circ$ , respectively, for HH polarization. The increased error of the SPM for HH polarization is expected

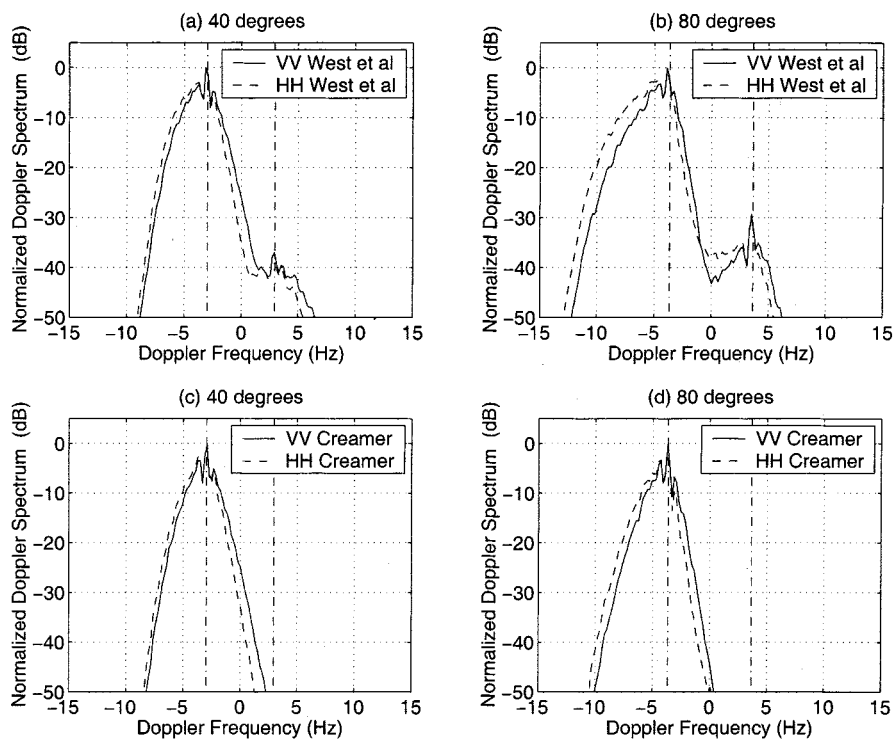


Fig. 7. Influence of polarization on Doppler spectra (a) the West model, 40°, (b) the West model, 80°, (c) Creamer model, 40°, and (d) Creamer model, 80°.

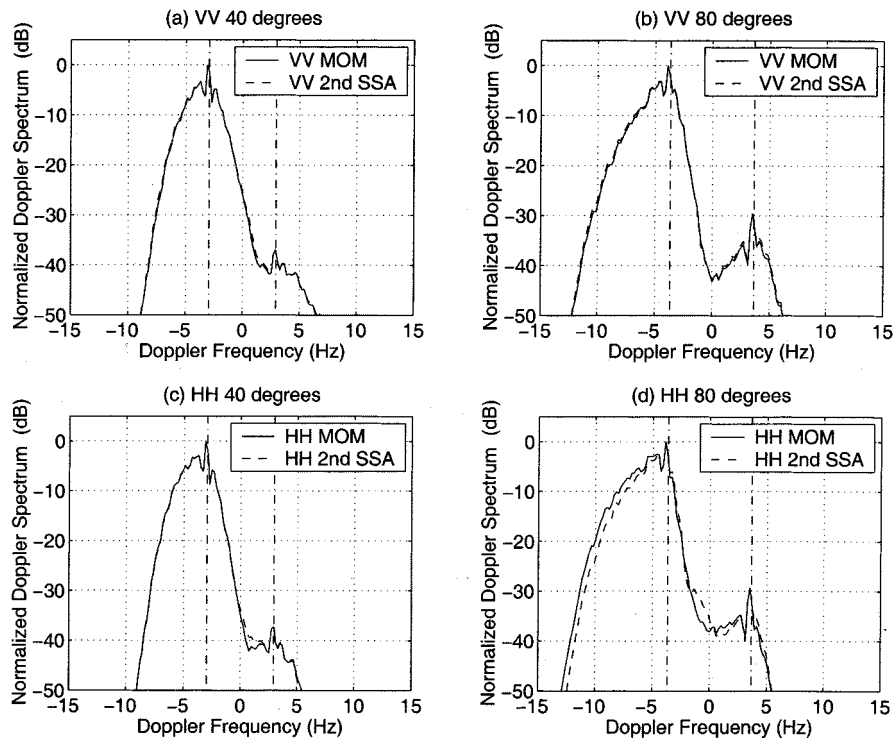


Fig. 8. Comparison of numerical and second order SSA scattering models for the West model Doppler spectra (a) VV, 40°, (b) VV, 80°, (c) HH, 40°, and (d) HH, 80°.

for ocean-like surfaces which include some “long wave” features. Histograms of scattered fields for all models were found to be well fit by standard Rayleigh statistics (Ricean at 0° incidence where a coherent backscattered field exists).

Figs. 3–5 illustrate Doppler spectra normalized to unity peak value for zero, 40°, and 80° incidence, respectively. Results

from the three hydrodynamic models and for both VV and HH polarizations are included. Doppler spectra were obtained using the spectral estimation technique described in [5] with the 256 backscattered field time samples. Results in Fig. 3 at normal incidence show an almost precise match between the three models for this case, which is dominated by the

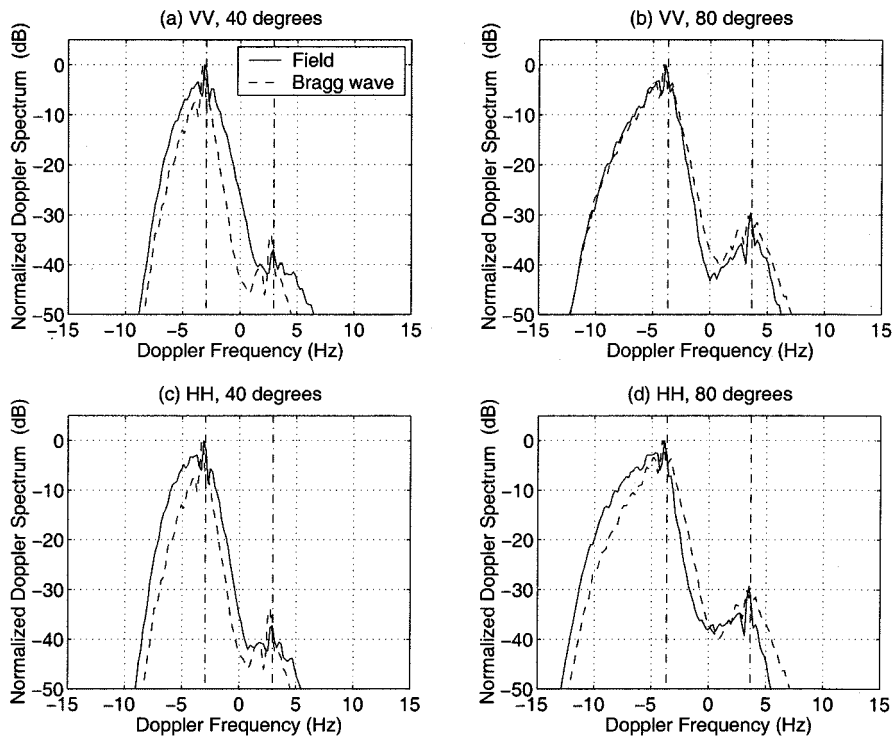


Fig. 9. Comparison of the West model backscattered field Doppler spectra and power spectral density of Bragg component (a) VV,  $40^\circ$ , (b) VV,  $80^\circ$ , (c) HH,  $40^\circ$ , and (d) HH,  $80^\circ$ .

specular reflection process. Larger differences are observed in Figs. 4 and 5, and a general trend of broader Doppler spectra is obtained from the linear to the Creamer model to the West model hydrodynamic models. This trend, along with the spectrum results of Fig. 2, seemingly indicates an increasing level of hydrodynamic interactions captured by the West model due to its inclusion of higher order nonlinear terms. Dotted lines in Figs. 4 and 5 indicate the locations of the Bragg frequencies, and all models obtain large values at these points. Table II compares first moments of the Doppler spectra as defined in [5] (the Doppler “centroid frequencies”) for the three hydrodynamic methods at incidence angles  $40^\circ$  and  $80^\circ$ , and includes the Bragg frequency values. As expected, results show increasing magnitudes of the centroid frequency from the linear to the Creamer model to West models.

Note the West model also obtains a smaller peak at the negative traveling Bragg frequency, indicating the presence of reverse traveling Bragg waves in the simulation. To determine whether these reverse going waves are created by the initial conditions and “ramp-up” period of the West model, Fig. 6 compares the West model, Doppler spectra at  $80^\circ$  for ramp parameters  $a = 1$  s,  $b = 0.376$  s, and  $a = 4$  s,  $b = 0.752$  s. Note the second case is a much longer and more gradual inclusion of nonlinear effects, so any reverse-going waves generated by the ramp function should be reduced. Since no strong effects on Doppler spectra are observed, it appears that these reverse going waves are a result of nonlinear interactions as the spectrum evolves.

Fig. 7 illustrates the dependence of Doppler spectra on polarization for the West model and Creamer model models at  $40^\circ$  and  $80^\circ$  incidence. The West model at  $80^\circ$  incidence is observed to produce the largest dependence on polarization, with the HH

Doppler spectrum somewhat broader than VV. The centroid frequencies of Table II also show larger amplitudes in HH polarization than in VV. Overall, polarization dependencies in the normalized Doppler spectra are relatively weak for the low wind speed case considered here. Note that the first order SPM and first order SSA theories both predict no polarization sensitivity for Doppler spectra; the dependencies captured by the numerical model demonstrate that these approximations neglect some polarization dependent scattering effects.

Fig. 8 investigates the performance of the second order SSA for scattering predictions. Results for the West model surfaces are illustrated in HH and VV polarizations. SSA results provide high accuracy in general, but slightly underestimate the width of the HH result at  $80^\circ$ . Comparisons using first order SSA predictions provide a similar level of agreement to that of Fig. 8 in VV polarization but further underestimate the width for HH polarization. Average radar cross sections from the second order SSA are within 1 dB of the values given in Table I for the West model model at all angles.

Finally, Fig. 9 illustrates a test of Bragg scattering theory by comparing Doppler spectra for the West model model with the average power spectral density of the corresponding Bragg wave component of the surface spectrum. Bragg wave components for a given surface realization were extracted from the surface Fourier transform at each time step. The similarities in Bragg wave and VV scattered field spectral densities at  $80^\circ$  incidence suggests that Bragg scattering is being observed for this case. The level of agreement at  $40^\circ$  and in HH polarization however shows that additional scattering effects are important for these cases. This comparison provides an example of the potential benefits of coupled electromagnetic and hydrodynamic simu-

lations, since both scattered fields and surface geometries can be examined in detail to clarify the scattering process.

## V. CONCLUSION

The results of this paper demonstrate the influence of the hydrodynamic model used on electromagnetic scattering results, and suggest that further assessments and extensions of current hydrodynamic models are necessary. The West model was found to capture a larger degree of surface nonlinearity and also to predict a slight presence of reverse traveling waves. However, the problems of the model with highly sloped features represent a serious limitation, as evidenced by the low wind speed limits of this paper. Methods for reducing these problems in the West model as well as studies with other hydrodynamic models [11] are currently under consideration for extending maximum wind speeds to more reasonable values. The advantages of coupled numerical hydrodynamic and electromagnetic simulations were also demonstrated, through detailed comparisons of scattered field and surface profile data which can assist in clarifying the scattering process. Improvements in understanding sea surface scattering will help to improve current remote sensing technologies and to design new sensors for the future.

## ACKNOWLEDGMENT

The authors would like to thank Prof. G. Baker of the Mathematics Department, The Ohio State University, Columbus, for helpful discussions and Mr. H. Kim for SSA calculations.

## REFERENCES

- [1] G. S. Brown, Ed., *IEEE Trans. Antennas Propagat., Special Issue on Low Grazing Angle Backscatter From Rough Surfaces*, vol. 46, Jan. 1998.
- [2] J. T. Johnson, R. T. Shin, J. A. Kong, L. Tsang, and K. Pak, "A numerical study of the composite surface model for ocean scattering," *IEEE Trans. Geosci. Remote Sensing*, vol. 36, pp. 72–83, Jan. 1998.
- [3] J. T. Johnson and H. T. Chou, "Numerical studies of low grazing angle backscatter from 1-D and 2-D impedance surfaces," in *Proc. IGARSS'98*, vol. 4, Seattle, WA, 1998, pp. 2295–2297.
- [4] C. L. Rino, T. L. Crystal, A. K. Koide, H. D. Ngo, and H. Guthart, "Numerical simulation of backscatter from linear and nonlinear ocean surface realizations," *Radio Sci.*, vol. 26, pp. 51–71, 1991.
- [5] J. V. Toporkov and G. S. Brown, "Numerical simulations of scattering from time varying, randomly rough surfaces," *IEEE Trans. Geosci. Remote Sensing*, vol. 38, pp. 1616–1625, July 2000.
- [6] B. Urgan and J. T. Johnson, "Time statistics of propagation over the ocean surface: A numerical study," *IEEE Trans. Geosci. Remote Sensing*, vol. 38, pp. 1626–1634, July 2000.
- [7] D. B. Creamer, F. Henyey, R. Schult, and J. Wright, "Improved linear representation of ocean surface waves," *J. Fluid Mech.*, vol. 205, pp. 135–161, 1989.
- [8] B. J. West, K. Brueckner, R. Janda, D. Milder, and R. Milton, "A new numerical method for surface hydrodynamics," *J. Geophys. Res.*, vol. 92, pp. 11 803–11 824, 1987.
- [9] A. G. Voronovich, *Wave Scattering from Rough Surfaces*. Berlin, Germany: Springer-Verlag, 1994.
- [10] M. S. Longuet-Higgins and E. Cokelet, "The deformation of steep surfaces waves on water I: A numerical method of computation," in *Proc. Royal Society*, vol. 350, London, U.K., 1976.
- [11] G. R. Baker, D. Meiron, and S. Orszag, "Generalized vortex methods for free surface flow problems," *J. Fluid Mech.*, vol. 123, pp. 477–501, 1982.

- [12] K. M. Watson and B. J. West, "A transport equation description of nonlinear ocean surface wave interactions," *J. Fluid Mech.*, vol. 70, pp. 815–826, 1975.
- [13] D. G. Dommermuth and D. K. P. Yue, "A high-order spectral method for the study of nonlinear gravity waves," *J. Fluid Mech.*, vol. 184, pp. 267–288, 1987.
- [14] W. H. Press, S. A. Teukolsky, W. T. Vetterling, and B. P. Flannery, *Numerical Recipes: The Art of Scientific Computing*, 2nd ed. New York: Cambridge Univ. Press, 1992.
- [15] D. G. Dommermuth, "The initialization of nonlinear waves using an adjustment scheme," *Wave Motion*, vol. 32, pp. 307–317, 2000.
- [16] D. M. Milder, H. T. Sharp, and R. A. Smith, "Numerical Simulation of Ultra-Wideband Microwave Backscatter from the Wind Roughened Sea Surface," Tech. Rep. AU-94-005, Arete Assoc., Sherman Oaks, CA, 1994.
- [17] "Maui High Performance Computing Center," [Online] Available: [www.mhpc.edu](http://www.mhpc.edu).
- [18] D. A. Kapp and G. S. Brown, "A new numerical method for rough-surface scattering calculations," *IEEE Trans. Antennas Propagat.*, vol. 44, pp. 711–721, May 1996.
- [19] H. T. Chou and J. T. Johnson, "A novel acceleration algorithm for the computation of scattering from rough surfaces with the forward-backward method," *Radio Sci.*, vol. 33, no. 5, pp. 1277–1287, 1998.
- [20] —, "Formulation of forward-backward method using novel spectral acceleration for the modeling of scattering from impedance rough surfaces," *IEEE Trans. Geosci. Remote Sensing*, pt. II, vol. 38, pp. 605–607, Jan. 2000.
- [21] J. V. Toporkov, R. Awadallah, and G. S. Brown, "Issues related to the use of a Gaussian-like incident field for low-grazing-angle scattering," *J. Opt. Soc. Amer. A*, vol. 16, no. 1, pp. 176–187, 1999.
- [22] L. A. Klein and C. T. Swift, "An improved model for the dielectric constant of sea water at microwave frequencies," *IEEE Trans. Antennas Propagat.*, vol. AP-25, pp. 104–111, 1977.
- [23] S. L. Broschat and E. I. Thorsos, "An investigation of the small slope approximation for scattering from rough surfaces 2: Numerical studies," *J. Acoust. Soc. Amer.*, vol. 101, no. 5, pp. 2615–2625, 1997.
- [24] S. T. McDaniel, "Acoustic and radar scattering from directional seas," *Waves Random Media*, vol. 9, no. 4, pp. 537–549, 1999.
- [25] T. Elfouhaily, D. R. Thompson, D. Vandemark, and B. Chapron, "A new bistatic model for electromagnetic scattering from perfectly conducting random surfaces," *Waves Random Media*, vol. 9, no. 3, pp. 281–294, 1999.
- [26] J. V. Toporkov and G. S. Brown, "Numerical study of the extended Kirchhoff approach and the lowest-order small slope approximation for scattering from ocean-like surfaces: Doppler analysis," *IEEE Trans. Antennas Propagat.*, to be published.
- [27] A. G. Voronovich, "Small slope approximation and a two-scale model," in *Proc. IEEE Antennas Propagat. Soc./URSI Symp. URSI B Conf.*, 2001, p. 243.
- [28] D. R. Thompson, B. L. Gotwols, and W. C. Keller, "A comparison of Ku-band Doppler measurements at 20 degrees incidence with predictions from a time-dependent scattering model," *J. Geophys. Res.*, vol. 96 C3, pp. 4947–4955, 1991.
- [29] S. O. Rice, "Reflection of electromagnetic waves from slightly rough surfaces," *Commun. Pure Appl. Math.*, vol. 4, pp. 361–378, 1951.

**Joel T. Johnson** (S'91–M'96) received the B.S. degree in electrical engineering from the Georgia Institute of Technology, Atlanta, in 1991, and the S.M. and Ph.D. degrees from the Massachusetts Institute of Technology, Cambridge, in 1993 and 1996, respectively.

He is currently an Associate Professor in the Department of Electrical Engineering and ElectroScience Laboratory, The Ohio State University, Columbus. His research interests are in the areas of microwave remote sensing, propagation, and electromagnetic wave theory.

Dr. Johnson is a member of commissions B and F of the International Union of Radio Science (URSI), and a member of Tau Beta Pi, Eta Kappa Nu, and Phi Kappa Phi. He received the 1993 Best Paper Award from the IEEE Geoscience and Remote Sensing Society and was named an Office of Naval Research Young Investigator, National Science Foundation Career Awardee, and PECASE award recipient in 1997.

**Jakov V. Toporkov** (A'98) was born in Sverdlovsk (now Yekaterinburg), Russia, in 1966. He received the M.S. degree (with distinction) in electronics engineering from the Moscow Institute of Physics and Technology, Moscow, Russia, in 1989, and the M.S. and Ph.D. degrees in physics from Virginia Polytechnic Institute (Virginia Tech), Blacksburg, in 1996 and 1998, respectively.

From 1989 to 1993, he was employed in Russia as an Engineer-Researcher, involved in the design of synthetic aperture radar (SAR). In particular, his research interests at the time included SAR imaging of moving targets. From 1998 to 1999, he held a Postdoctoral appointment at the Bradley Department of Electrical and Computer Engineering at Virginia Tech, where he worked on the numerical studies of scattering from randomly rough ocean-like surfaces. Currently, he is a Senior Engineer with SFA, Inc., Largo, MD, and is stationed at the Naval Research Laboratory, Washington, DC. There he is engaged in the development of image processing capabilities for ultrawideband light airborne SAR systems and in studies of scattering from ocean surfaces. His present research interests include electromagnetic scattering by randomly rough surfaces at low grazing angles and SAR remote sensing.

Dr. Toporkov is a member of Commission F of the U.S. National Committee of the International Union of Radio Science (USNC-URSI). In 1999, together with his co-authors R. Marchand and G. Brown, he was a recipient of the IEEE Antennas and Propagation Society Schelkunoff Best Paper Award.

**Gary S. Brown** (M'67–SM'81–F'86) was born in Jackson, MS, on April 13, 1940. He received the B.S., M.S., and Ph.D. degrees from the University of Illinois, Urbana, all in electrical engineering.

From 1963 to 1967, he was a Research Assistant in the old Antenna Laboratory, University of Illinois, where he was involved with direction finding, shaped beam antennas, and millimeter waveguides. While in the U.S. Army Signal Corps from 1967 to 1969, he served in an engineering capacity, dealing with the Integrated Wideband Communications System (IWCS) in the Republic of Vietnam. In 1970, he was employed by TRW Systems Group, Redondo Beach, CA, where his work involved monopulse, ECM, and multiple-beam antenna analysis and development. From 1971 to 1973, he was with the Research Triangle Institute, Research Triangle Park, NC, where his primary area of interest was spaceborne radar altimetry. From 1973 to 1985, he was employed by Applied Science Associates, Inc., Apex, NC, where he worked with microwave remote sensing, rough surface scattering, and propagation through random media. In 1985, he joined the faculty of Virginia Polytechnic Institute, Blacksburg, where he is presently Director of the ElectroMagnetic Interactions Laboratory (EMIL). His primary area of interest focuses on the interaction of electromagnetic waves with the natural environment.

Dr. Brown is a member of Commissions B (Fields and Waves) and F (Propagation in Non-Ionized Media and Remote Sensing) of the U.S. National Committee of the International Union of Radio Science (USNC-URSI) and is presently Chair of USNC-URSI. He was President of the Antennas and Propagation Society in 1988 and received the R.W.P. King Award in 1978 and the Schelkunoff Best Paper Award with J. Toporkov and R. Marchand in 1999. He has served on a number of IEEE award committees.